Journal of Materials Chemistry A

Accepted Manuscript

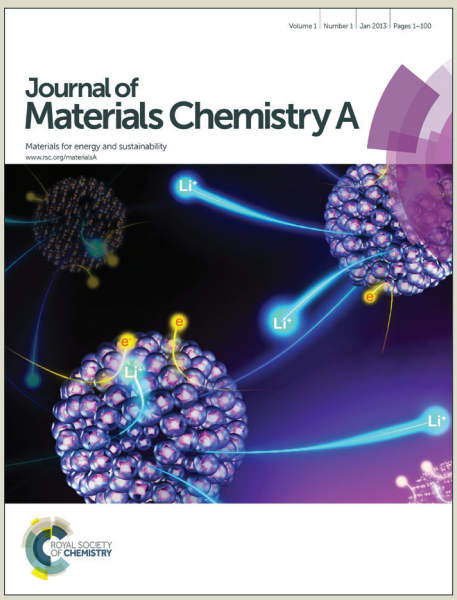

This is an *Accepted Manuscript*, which has been through the Royal Society of Chemistry peer review process and has been accepted for publication.

Accepted Manuscripts are published online shortly after acceptance, before technical editing, formatting and proof reading. Using this free service, authors can make their results available to the community, in citable form, before we publish the edited article. We will replace this *Accepted Manuscript* with the edited and formatted *Advance Article* as soon as it is available.

You can find more information about *Accepted Manuscripts* in the Information for Authors.

Please note that technical editing may introduce minor changes to the text and/or graphics, which may alter content. The journal's standard Terms & Conditions and the Ethical guidelines still apply. In no event shall the Royal Society of Chemistry be held responsible for any errors or omissions in this *Accepted Manuscript* or any consequences arising from the use of any information it contains.

ROYAL SOCIETY OF CHEMISTRY

www.rsc.org/materialsA

Large-scale synthesis of Si@C three-dimensional porous structures as high-performance anode materials for lithium-ion batteries

Chengmao Xiao[a], Ning Du[a*], Xianxing Shi[b], Hui Zhang[a], Deren Yang[a]

[a] State Key Lab of Silicon Materials and Department of Materials Science and Engineering, Cyrus Tang Center for Sensor Materials and Applications, Zhejiang University, Hangzhou 310027, People's Republic of China

[b] Wanxiang A123 Systems Asia Co., Ltd.

Abstract

We demonstrate the synthesis of the Si@C three-dimensional porous structures derived from commercial magnesium silicide (Mg_2Si) powders via simple annealing and acid pickling processes. When used as anode materials of lithium-ion batteries, the Si@C three-dimensional porous structures can give more lithiation sites and accommodate large volume changes during the lithiation/delithiation process, which leads to high capacity and good cycling stability. As a result, a high reversible capacity of ~1700 $mAhg^{-1}$ was obtained at a current of 0.2 C (800 mAg^{-1}, 1C = 4 Ag^{-1}) even after 70 cycles. The synthetic route described herein is a low-cost and large-scale way to produce high-performance Si anodes, which may facilitate the commercial application.

Introduction

Lithium-ion batteries (LIBs) have been motivated to high energy density and high volumetric density due to the rapidly increasing demand in electronics consumer especially in electronic vehicles [1]. Graphite-based materials are commonly used as anode materials in most commercial LIBs due to their advantages such as low cost, high yield and long cycle life. However, their limited gravimetric capacity (372 mAh

*Author to whom correspondence should be addressed; electronic mail: dna1122@zju.edu.cn, tel: 86-571-87953190, fax: 86-571-87952322.

Journal of Materials Chemistry A Accepted Manuscript

g^{-1}) has prompted intensive research for alternative anode materials with large capacity at low potentials. Recently, some new anode materials with high specific capacity such as tin (Sn) [2-3], transitional oxide materials [4-5], silicon (Si) [6-8] and germanium (Ge) [9-10] have been pursued. Particularly, Si has attracted much attention due to the advantages such as the highest theoretic capacity of 4200 $mAhg^{-1}$, the low discharge potential (0.37 mV vs. Li/Li^+), non-toxic, and abundant reserves [11-12]. However, the large volume changes (>300%) during the lithiation/de-lithiation process brings cracking and crumbling of the Si anodes, which results in the capacity fades and poor cycling life [13].

Tremendous efforts have been devoted to improve the cycling performance of Si anodes. Typically, there are two strategies. The first is the design of composite materials in which Si dispersing in a matrix [14-15]. The matrix is used to buffer the stress induced by the volume expansion and enhance the conductivity. The other strategy is the design of the nano/miro-structure of Si materials such as nanoparticle [16], thin film [17-18], nanotubes or nanowires [19-22] and porous structures [23-24], which can sustain the physical stains during the lithiation/de-lithiation process. Among them, the porous Si structure is the hot spot because of its pores and relative large surface area, which can enhance the diffusion of lithium ions and accommodate the volume change. Many methods, such as chemical etching [25-29], template-assisted [30-31], and magnesium reduction process [32-36] have been reported to synthesize the porous Si materials. For example, Bang et al. used a displacement reaction and metal-assisted chemical etching method to synthesize porous Si particles, which exhibited good cycling performance and high capacity [26]. However, the expensive Ag is used for etching and the productivity is relatively low, which limits its further application. Yu et al. synthesized Si porous particle via a magnesiothermic reduction between Mg powder and mesoporous SiO_2 particles [32]. In order to obtain the good cycling performance, Ag coating was further deposited onto the Si porous particles. In this case, the pre-synthesized mesoporous SiO_2 particles were used as source and expensive Ag was coating on the porous Si particles, indicating that the commercial production is difficult. Therefore, the exploration of

Journal of Materials Chemistry A Accepted Manuscript

large-scale, low-cost and convenient way for industrial production of porous Si materials is a great challenge.

Herein, we use the commercial Mg_2Si as the source to prepare Si@C three-dimensional porous structures (TPS) via simple annealing and acid washing processes, which can act as the high-performance anode materials of LIBs. There are three main progress compared to the above-mentioned methods for porous Si materials: the first is the use of commercial Mg_2Si as source with a low price of ~5 \$/kg; the second is the simple annealing and acid washing process, which is suitable for large-scale production; the last is that the carbon coating process has been integrated in the simple annealing process which is more suitable for large production compared to the previous reported acetylene decomposition [25-26, 30].

Experimental procedure

Synthesis of the Si@C TPS

Mg_2Si (purity, >97%) was synthesized via a home-built continuous preparing apparatus using Si (purity, >98%) and Mg (purity, >99%) powder as sources. The Si@C TPS were successfully synthesized via the following procedures. At first, Mg_2Si, Polyvinyl alcohol (PVA), ethanol and grinding balls with a mass ratio of 1:1:2:6 was ground in a planetary ball mill (QM-3SP2, Nanjing University Instrument Company of China) at 500 rpm for 4 h. The ball-milled mixture was dried in the vacuum oven at 80 ^{o}C for 5 h. Then, the ball-milled mixture was heated to 350 ˚C for 5 h and raised to 700 ^{o}C at a heating rate of 5 ^{o}C min^{-1} under a mix gas (N_2 : air = 20:1) atmosphere, for another 12 h in a rotary furnace (XY-1700S, XINYOO, Nan Yang Xin YU Electric Components CO., Ltd. of China). After cooling down to room temperature, the powder was washed with HF (5%) and HCl (0.2 molL^{-1}) to remove the MgO and SiO_2. Final product was achieved by centrifuged in deionized water and alcohol for three times, and then dried in the vacuum oven at 80 ^{o}C for 12 h. For comparison, bare Si TPS without carbon layer were synthesized in the same procedure in absence of polyvinyl alcohol (PVA).

Characterization of the products

The crystal structure of the products were identified by a high power X-ray

Journal of Materials Chemistry A Accepted Manuscript

diffraction (XRD) using a Rigaku D/max-ga X-ray diffractometer with graphite monochromatized Cu Kα radiation (λ = 1.54 Å). The morphology and structure of the products were evaluated by scanning electron microscopy (SEM HITACH S4800) and Transmission electron microscopy (TEM, PHILIPS F200). Thermogravimetric analysis (TGA) was tested on SDT Q600 V8.2 Bulid 100. Brunauer-Emmertt-Teller (BET) surface area and pore volume were tested using a Beckman Coulter Omnisorp100cx. The Raman experiments were performed with a HR800 Raman spectrometer using the 514 nm line of an Ar ion laser operated at 10 mW.

The electrochemical performance of the Si@C TPS

The electrochemical properties of coin-type half cells (2016 R-type) composed of the Si@C TPS as the working electrode and lithium metal as the counter electrode were tested. The working electrode was made of the Si@C TPS, poly(vinylidenefluoride) (PVDF) as the binder, acetylene black (AB) as the conductive additive in a weight rate of 70:15:15. The uniform slurry was obtained after dissolving the three materials in the N-methyl-2pyrrolidine (NMP). Then the slurry was pasted on the copper foils. After dried in the vacuum at 120 ^{o}C for 12 h, the half cells were assembled in a glovebox (Mbraun, Labstar, Germany) under argon atmosphere, where the electrolyte solution was composed of 1M $LiPF_6$ in ethylene carbonate/dimethyl carbonate (EC/DMC,1:1 in volume). Charge and discharge were conducted at the potentials between 0.001 and 2 V at different current densities. Cyclic Voltammetry (CV) of the same potential range was recorded on an Arbin BT2000 system at a scanning rate of 0.1 mVs^{-1}.

Results and discussion

The Si@C TPS were derived from Mg_2Si/PVA composites at 700 ^{o}C in a rotary tubular furnace under nitrogen/air (20:1) atmosphere and subsequent acid pickling (**Figure 1a**). A small amount of oxygen is necessary for the oxidation of Mg, while too much oxygen will bring the excessive oxidation of Si and negative influence on carbon layer. Therefore, an appropriate ratio of nitrogen/air (20:1) is necessary for the synthesis of the Si@C TPS. Mg_2Si is a commercial raw material for silane (SiH_4) in Komatsu method, which can decompose to Mg and Si at high temperature. Mg, whose

Journal of Materials Chemistry A Accepted Manuscript

melting point is 648 ^{o}C, is very active and can be oxidized fast even under a little oxygen, resulting in the formation of MgO. At the same time, PVA can be converted to the carbon layer under the similar conditions. Therefore, the Si@C TPS were obtained after acid pickling and drying in vacuum (**Figure 1b**). It can be seen that the surface of the initial Mg_2Si particles is smooth (**Figure 1c**), which transforms into porous structure (**Figure 1d**) due to the removal of MgO after the annealing and acid pickling process.

The synthetic process can be further identified by the XRD patterns (**Figure 2**) .The peaks of the raw material is consistent with the cubic Mg_2Si (JCPDS no. 01-075-0445). After the annealing process, the peaks of Mg_2Si disappear instead of MgO and Si, indicating the transformation from Mg_2Si to MgO and Si. It should be mentioned that PVA has been converted into carbon, which can not reflect in the XRD pattern due to the amorphous nature. After the acid pickling process, only the peaks of Si can be observed, indicating the complete removal of MgO. The yield of this process is nearly 30 %, which is much higher than the previous results for porous Si materials (<10 %) [23, 37].

Figure 3 shows the morphological and compositional characterization of the as-synthesized products. It can be seen from **Figure 3a** that the products show the morphology of three-dimensional structures with the size range from several micrometers to tens of micrometers. From the magnified SEM image (**Figure 3b**), it can be seen that the pores with several tens to hundreds nanometers distribute randomly in a whole Si microparticle, which is due to the elimination of MgO. **Figure 3c** shows the high-resolution TEM image of an individual Si microparticle. It is observed that a carbon layer with a thickness of ~20 nm has deposited onto the Si particle, which comes from PVA in the raw material. To further confirm the carbon layer, Raman test was employed (**Figure 3d**). In addition to the peak of Si at 940 cm^{-1}, two typical peaks at ~1340 cm^{-1} (D band) and ~1580 cm^{-1}(G band) represent the amorphous carbon layer [24, 25]. To further confirm the content of the carbon in the Si@C TPS, TGA analysis was employed (**Figure 4**). As can be seen, the Si@C TPS show slow mass fading from 50 to 350 ºC, which may be attributed to the loss of

Journal of Materials Chemistry A Accepted Manuscript

crystal water. Then, a fast mass fading is observed between 480 ºC and 620 ºC, following with a stable zone in the higher temperature. It can be estimated that the amount of the carbon is 14.8 %. BET analysis was employed to estimate the porosity of the Si@C TPS (**Figure 5**). It can be seen that the Si@C TPS have a BET surface area of 41.9 m^2g^{-1} with an average Barretl-Joyner-Halenda (BJH) pore diameter of ~40 nm, which further confirm the porous structure. The porous structure can facilitate the fast lithium ion diffusion and accommodate the volume change during the lithiation/delithiation process, leading to the enhanced performance.

For comparison, bare Si TPS without the carbon layer were synthesized via the same process in absence of the carbon source (PVA). **Figure 6** shows the morphological and compositional characterization of as-synthesized products. It can be seen that the products show the morphology of porous microparticles with pores distributed randomly in the entire Si particles (**Figures 6a-c**). Compared to Si@C, Si seems more porous, and the distribution and diameters of the pores is more uniform because of the absence of the carbon layer. **Figure 6d** shows the EDX pattern of the as-synthesized bare Si TPS. As can be seen, the EDX pattern shows the peaks of Si and Cu, which come from the products and Cu substrate for SEM sample, respectively, indicating the complete removal of MgO and absence of carbon layer. It should be mentioned that the BET surface area of bare Si TPS is 94.16 m^2g^{-1}, which is larger than the Si@C TPS because the carbon layer may cover some pores during the annealing process.

Motivated by the unique three-dimensional porous structures, the products were tested as the anode materials of LIBs. **Figure 7a** shows the CV curves for the Si@C TPS with a potential range of 0.001~2 V (*vs.* Li^+/Li) at a scanning rate of 0.1 mVs^{-1}. In the first cycle, a cathodic peak appears at ~0.2 V and becomes quite large in the following cycles, which is ascribed to the insertion of the lithium ions to form a series of Li_xSi. This is consistent with the previous report [39]. In the anodic process, two broad peaks at ~0.4 and 0.5 V represent the delithiation process. After the first cycle, all the peaks correspond to the phase transition between the amorphous Li_xSi and Si, which are the typical Si anodic peaks. In addition, the shapes of the 2^{nd} and 3^{rd} cycles

Journal of Materials Chemistry A Accepted Manuscript

are almost the same, suggesting the high reversibility of the following lithiation/delithiation process. To illustrate the advantage of the three-dimensional porous structures, the cycling performance of the bulk Si particles, the bulk Si@C particles, bare Si TPS, and Si@C TPS has been compared (**Figure 7b)**. It should be mentioned that the size of the bulk Si particles similar to the porous Si particles is chosen to guarantee the consistency of the comparison. It can be seen that the bulk Si shows rapid capacity fade, resulting in a capacity of 200 $mAhg^{-1}$ just after 10 cycles. After the coating of carbon layer, the cycling performance can be improved to a limited extent because the large volume expansion may still destroy the carbon layer and the core-shell structure can't be retained after the lithiation process. Similarly, the bare Si TPS also show the poor cycling performance, indicating that the carbon layer is necessary for retaining the porous structure during the lithiation/delithiation process. For comparison, the Si@C TPS show almost no capacity fading and a high capacity of ~1900 $mAhg^{-1}$ is achieved after 15 cycles at 0.1 C, which is extremely better than the other three samples. This result indicates that the porous structure and carbon layer are both important for the stability of the structure during the lithiation/delithiation process. The porous structure can allow the volume expansion inward and outward at the same time, while the carbon layer can prevent the excessive expansion outerward. **Figure 7c** shows the voltage profiles of the Si@C TPS anode at 0.1 C between 0.001 and 2 V. The first discharge and charge capacities are 2240 and 1860 $mAhg^{-1}$, indicating an initial Coulombic efficiency of 83 %. The first Coulombic efficiency is much higher than bulk Si/C composites [34] and similar to the previous porous Si materials [23, 25]. After the first cycle, the Coulombic efficiency shows a value higher than 97% in the second cycle and nearly 99% in the following cycles. Moreover, the discharge capacity maintains to over 1700 $mAhg^{-1}$ after 70 cycles at 0.2 C, indicating the good cycling performance (**Figure 7d**). It should be mentioned that the purity of the Si@C TPS is limited due to the limited purity of commercial Mg_2Si (96%). Considering that the source materials are chemically pure at least in the previous reports [25-36], the performance of the Si@C TPS is outstanding. For further evaluate the effect of the carbon layer, we have also

Journal of Materials Chemistry A Accepted Manuscript

tested the Si@C TPS with low carbon content (~8%) for 100 cycles under the same testing condition (**Figure 8**). It can be seen that the initial discharge capacity of the Si@C TPS with low carbon content is much higher than that with higher carbon content because the theoretic capacity of carbon is low. But the capacity of the sample with low carbon content decrease gradually along with the cycles, indicating that the thicker carbon layer can stabilize the structure better during the charge/discharge process. We can conclude from the comparison of Figure 8 and 7d that the high carbon content can facilitate the cycling performance. It should be mentioned that the variation trend of the capacity versus cycle numbers is steady after 70 cycles.

In order to confirm the stability of the three-dimensional porous structure during the lithiation/delithiation process, the morphological of the bulk Si, bare Si TPS, and Si@C TPS before and after cycling was characterized (**Figure 9**). It can be seen that the structure of the Si@C TPS can be retained after cycling, while the bulk Si and bare Si TPS seems broken and pulverizing. It can be concluded that the structure of the Si@C TPS is more stable than the bulk Si and bare Si TPS, which can also explain the enhanced cycling performance of the Si@C TPS.

Conclusions

In summary, the Si@C TPS were derived from commercial Mg_2Si powder via simple annealing and acid pickling processes. When used as anode materials of LIBs, the Si@C TPS show a high reversible discharge capacity of over 1700 $mAhg^{-1}$ after 70 cycles at 0.2 C. The as-synthesized Si@C TPS show higher capacity and better cycling performance than the bulk Si@C and bare Si TPS. The porous structures could allow the volume expansion inward and outerward at the same time, and give more lithiation sites, while the carbon layer could stabilize the porous structure and the SEI film during the lithiation/delithiation process, which should be responsible for the enhanced performance. This result may facilitate the commercial application of Si-based anode materials for LIBs.

Acknowledgment

The authors would like to appreciate the financial supports from the 863 Project (No. 2011AA050517), Natural Science Foundation of China (No. 51002133),

Journal of Materials Chemistry A Accepted Manuscript

Zhejiang Provincial Natural Science Foundation of China (LY13E020003) and the Fundamental Research Funds for the Central Universities.

Notes and references

[1] J. Tarascon and M. Armand, *Nature* 2001, **414**, 359-367.

[2] G. Derrien, J. Hassoun, S. Panero, B. Scrosati, *Adv. Mater.* 2007, **19**, 2336-2340.

[3] S. Han, B. Jang, T. Kim, S. M. Oh and T. Hyeon, *Adv. Funct. Mater.* 2005, **15**, 1845-1850.

[4] J. Chen, L. Xu, W. Li, X Gou, *Adv. Mater.* 2005, **17**, 582-586.

[5] X. Zhu, Y. Zhu, S. Murali, M. Stoller, R. Ruoff, *ACS Nano* 2011, **5**, 3333-3338.

[6] J. Guo and C. Wang, *Chem. Commun*. 2010, **46**, 1428-1430.

[7] S. Klankowski, R. Rojeski, B. Cruden, J. Liu, J. Wu and J. Li, *J. Mater. Chem. A* 2013, **1**, 1055-1064.

[8] J. Yoo, J. Kim, Y. Jung, K. Kang, *Adv. Mater.* 2012, **24**, 5452-5456.

[9] W. Li, Y. Yin, S. Xin, W. Song, Y. Guo, *Energy Environ. Sci.* 2012, **5**, 8007-8013.

[10] J. Wang, N. Du, H. Zhang, J. Yu, D. Yang, *J. Mater. Chem.* 2012, **22**, 1511-1515.

[11] A. Esmanski and G. Ozin, *Adv. Funct. Mater*. 2009, **19**, 1999-2010.

[12] A. Kohandehghan, P. Kalisvaart, M. Kupsta, B. Zahiri, B. Amirkhiz, Z. Li, E. Memarzadeh, L. Bendersky, D. Mitlin, *J. Mater. Chem. A* 2013, **1**, 1600-1612.

[13] L. Su, Z. Zhou, M. Ren, *Chem. Commun.* 2010, **46**, 2590-2592.

[14] C. Zhao, Q. Li, W. Wan, J. Li, J. Li, H. Zhou, D. Xu, *J. Mater. Chem.* 2012, **22**, 12193-12197.

[15] L. Ji and X. Zhang, *Energy Environ. Sci.* 2010, **3**, 124-129.

[16] D. Mazouzi, B. Lestriez, L. Roué, D. Guyomard, *Electrochem. Solid-State Lett.* 2009, **12**, A215-A218.

[17] C. Hwang, C. Lim, J. Yang, J. Park, *J. Power Sources* 2009, **194**, 1061-1067.

[18] T. Takamura, S. Ohara, M. Uehara, J. Suzuki, K. Sekine, *J. Power Sources* 2004, **129**, 96-100.

[19] T. Song, J. Xia, J. Lee, D. Lee, M. Kwon, J. Choi, J. Wu, S. Doo, H. Chang, W. Park, D. Zang, H. Kim, Y. Huang, K. Hwang, J. Rogers and U. Paik, *Nano Lett.* 2010, **10**, 1710-1716.

Journal of Materials Chemistry A Accepted Manuscript

[20] L. Cui, Y. Yang, C. Hsu, Y. Cui, *Nano Lett.* 2009, **9**, 3370-3374.

[21] T. Hwang, Y. Lee, B. Kong, J. Seo, J. Choi, *Nano Lett.* 2012, **12**, 802-807.

[22] R. Ruffo, S. Hong, C. Chan, R. Huggins, and Y. Cui, *J. Phys. Chem. C* 2009, **113**, 11390-11398.

[23] H. Kim, B. Han, J. Choo, J. Cho, *Angew. Chem. Int. Ed*. 2008, **47**, 10151-10154.

[24]J. Cho, *J. Mater. Chem.* 2010, **20**, 4009-4014.

[25] B. Bang, H. Kim, H. Song, J. Cho, S. Park, *Energy Environ. Sci.* 2011, **4**, 5013-5019.

[26] B. Bang, J. Lee, H. Kim, H. Song, J. Cho and S. Park, *Adv. Energy Mater.* 2012, **2**, 878-883.

[27] Y. Liu, B. Chen, F. Cao, H. Chan, X. Zhao and J. Yuan, *J. Mater. Chem*. 2011, **21**, 17083-10786.

[28] D. Kang, J. Corno, J. Gole, H. Shin, *J. Electrochem. Soc.* 2008, **155**, A276-A281.

[29] A. Hochbaum, D. Gargas, Y. Hwang, P. Yang, *Nano Lett.* 2009, **9**, 3550-3554.

[30] H. Jia, P. Gao, J. Yang, J. Wang, Y. Nuli, Z. Yang, *Adv. Energy Mater.* 2011, **1**, 1036-1039.

[31] C. Du, C. Gao, G. Yin, M. Chen, L. Wang, *Energy Environ. Sci*. 2011, **4**, 1037-1042.

[32] Y. Yu, L. Gu, C. Zhu, S. Tsukimoto, P. Aken, J. Maier, *Adv. Mater.* 2010, **22**, 2247-2250.

[33] D. Chen, X. Mei, G. Ji, M. Lu, J. Xie, J. Lu, J. Y. Lee, *Angew. Chem. Int. Ed.* 2012, **51**, 2409-2413.

[34] M. Wang, L. Fan, M. Huang, J. Li, X. Qu, *J. Power Sources* 2012, **219**, 29-35.

[35] L. Shen, X. Guo, X. Fang, Z. Wang, L. Chen, *J. Power Sources* 2012, **213**, 229-232.

[36] M. Liu, C. Li, H. Du, X. You, *Chem. Commun.* 2012, **48**, 4950-4952.

[37] Y. Sugiyama, H. Okamoto, T. Mitsuoka, T. Morikawa, K. Nakanishi, T. Ohta, H. Nakano, *J. Am. Chem. Soc.* 2010, **132**, 5946-5947.

[38] K. Seng, M. Park, Z. Guo, H. Liu, J. Cho, *Angew. Chem. Int. Ed.* 2012, **51**, 5657-5661.

Journal of Materials Chemistry A Accepted Manuscript

[39] Y. Zhang, X. Xia, X. Wang, Y. Mai, S. Shi, Y. Tang, C. Gu, J. Tu, *J. Power Sources* 2012, **213**, 106-111.

Journal of Materials Chemistry A Accepted Manuscript

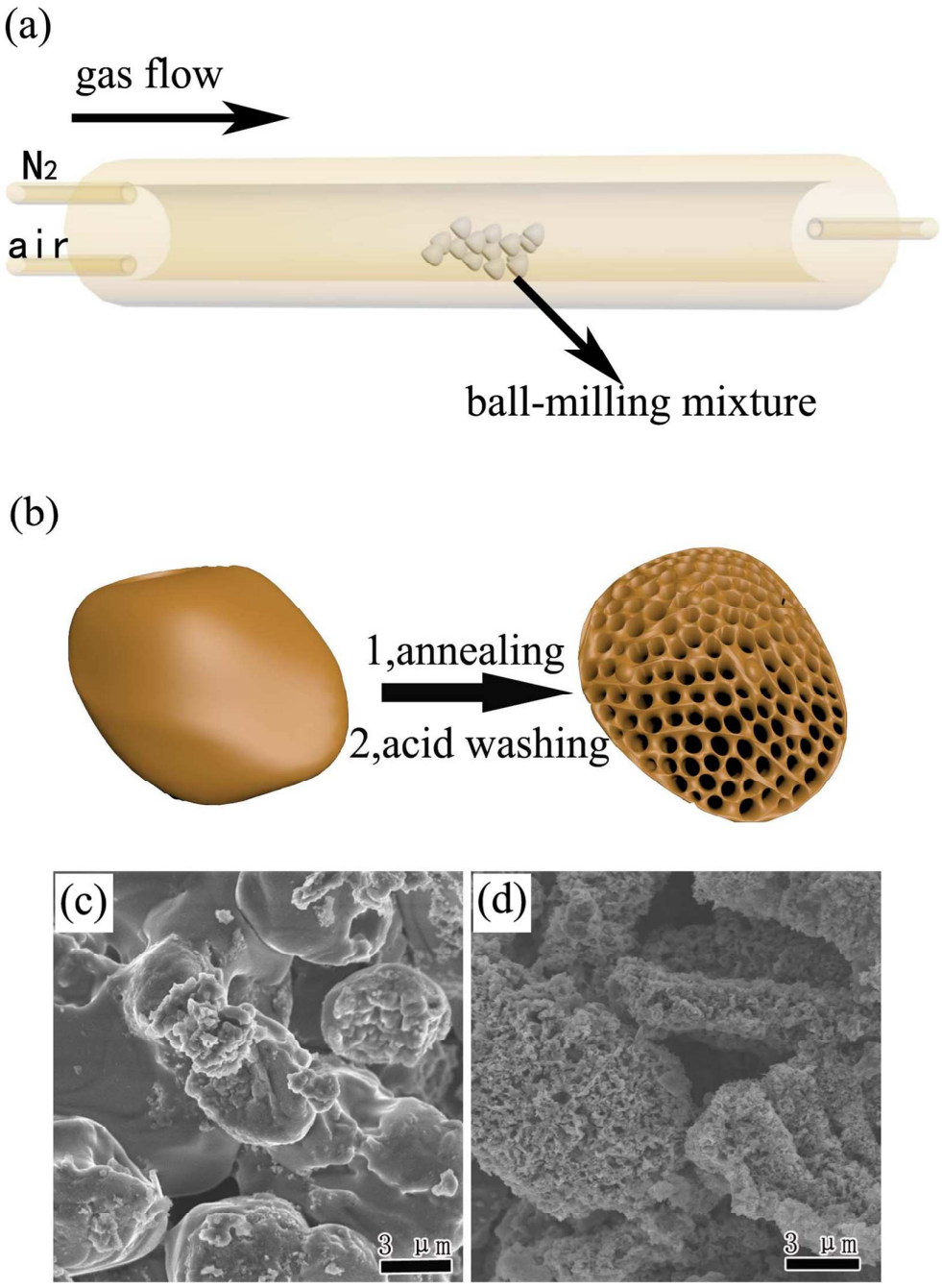

Figure 1. The schematic illustration (a), (b) and TEM images for the synthesis of Si TPS (c) derived from Mg_2Si (d).

Journal of Materials Chemistry A Accepted Manuscript

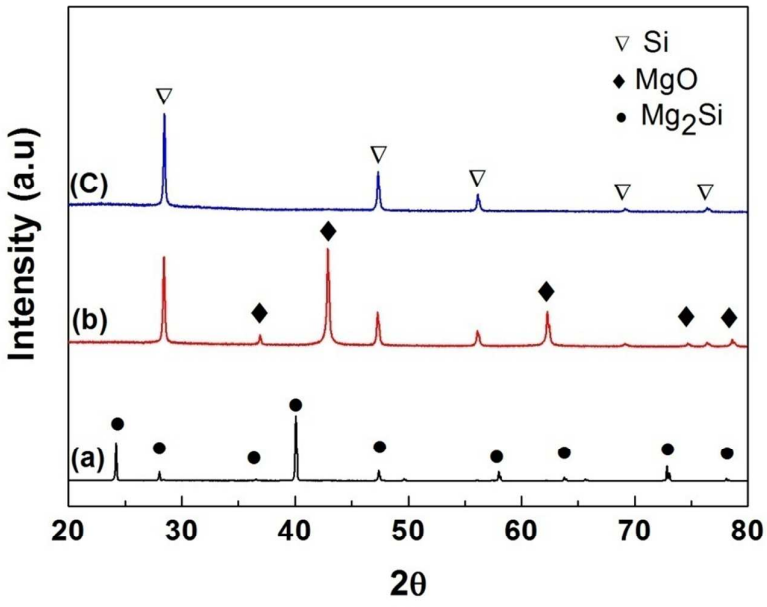

Figure 2. The evolutions of the XRD patterns from the raw Mg_2Si materials to the Si@C TPS

Journal of Materials Chemistry A Accepted Manuscript

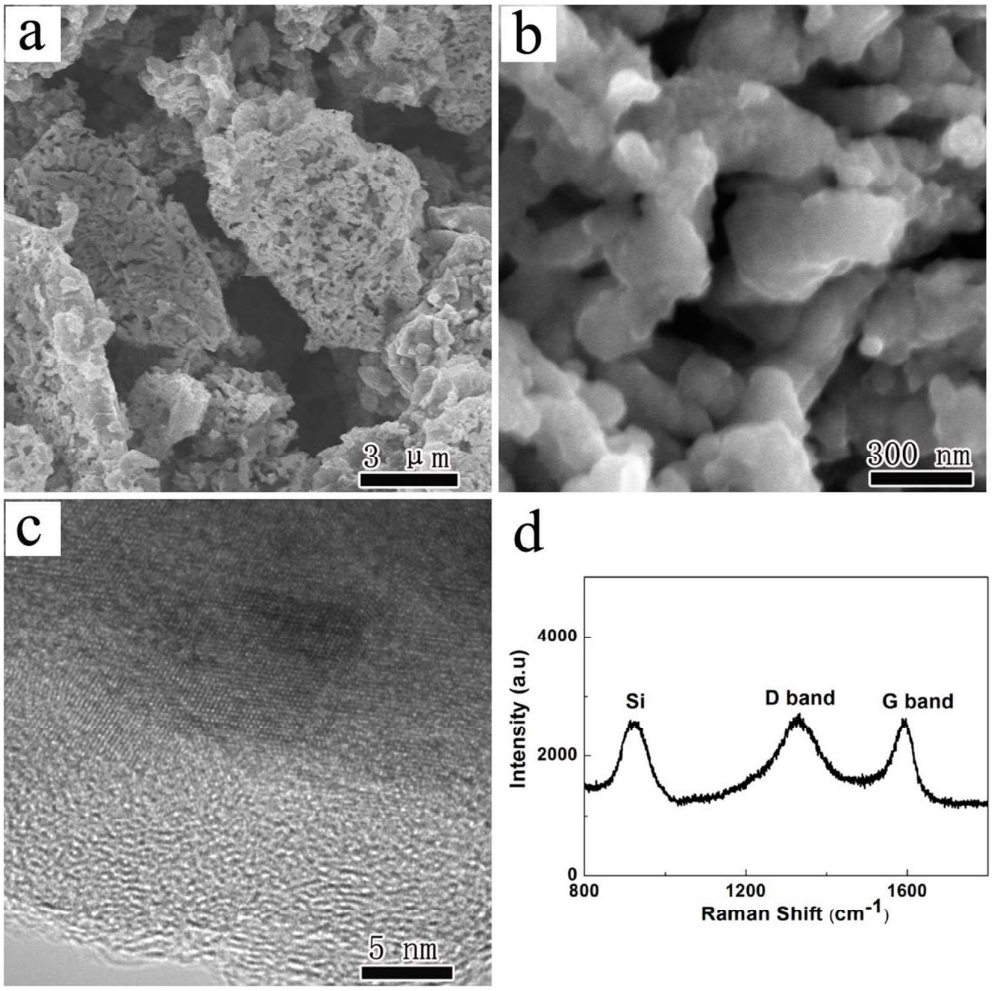

Figure 3. (a), (b) SEM images of the Si@C TPS at different magnification; (c) HRTEM image of the Si@C TPS;(d) Raman spectrum of the Si@C TPS

.

Journal of Materials Chemistry A Accepted Manuscript

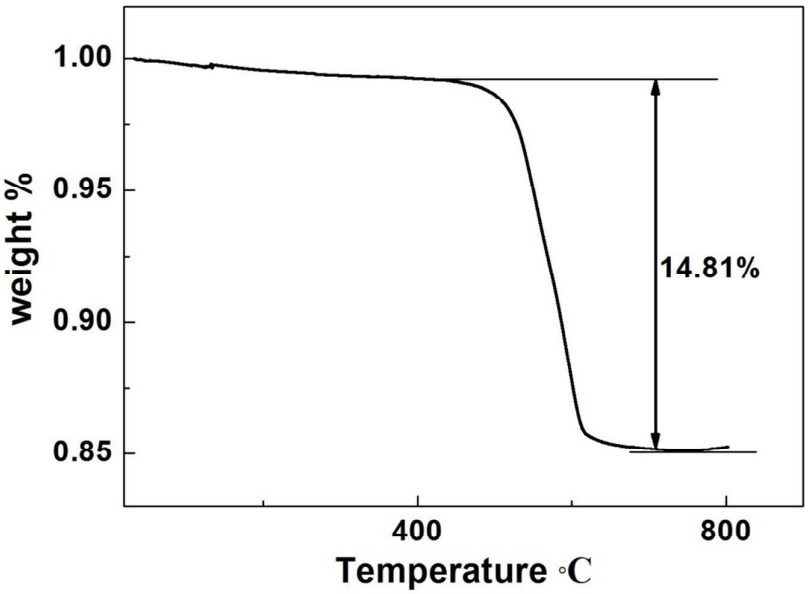

Figure 4. TGA analysis of the Si@C TPS

Journal of Materials Chemistry A Accepted Manuscript

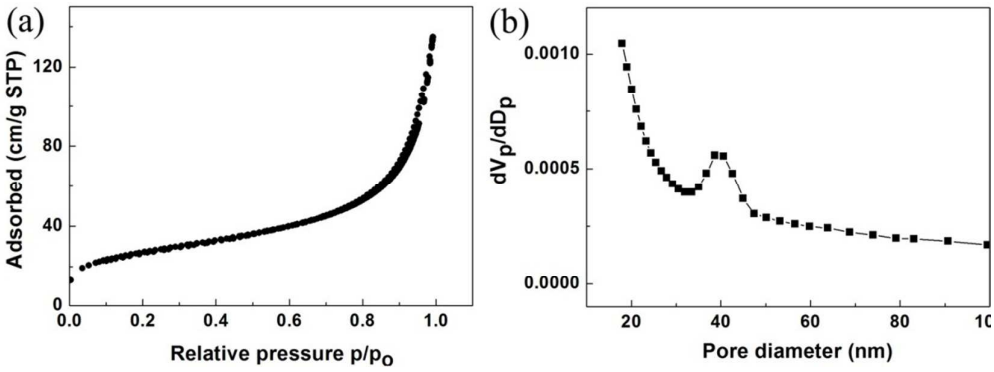

Figure 5. (a) Nitrogen adsorption and desorption isotherms of the Si@C TPS and (b) the corresponding pore-size distribution calculated by the BJH method from desorption branch

Journal of Materials Chemistry A Accepted Manuscript

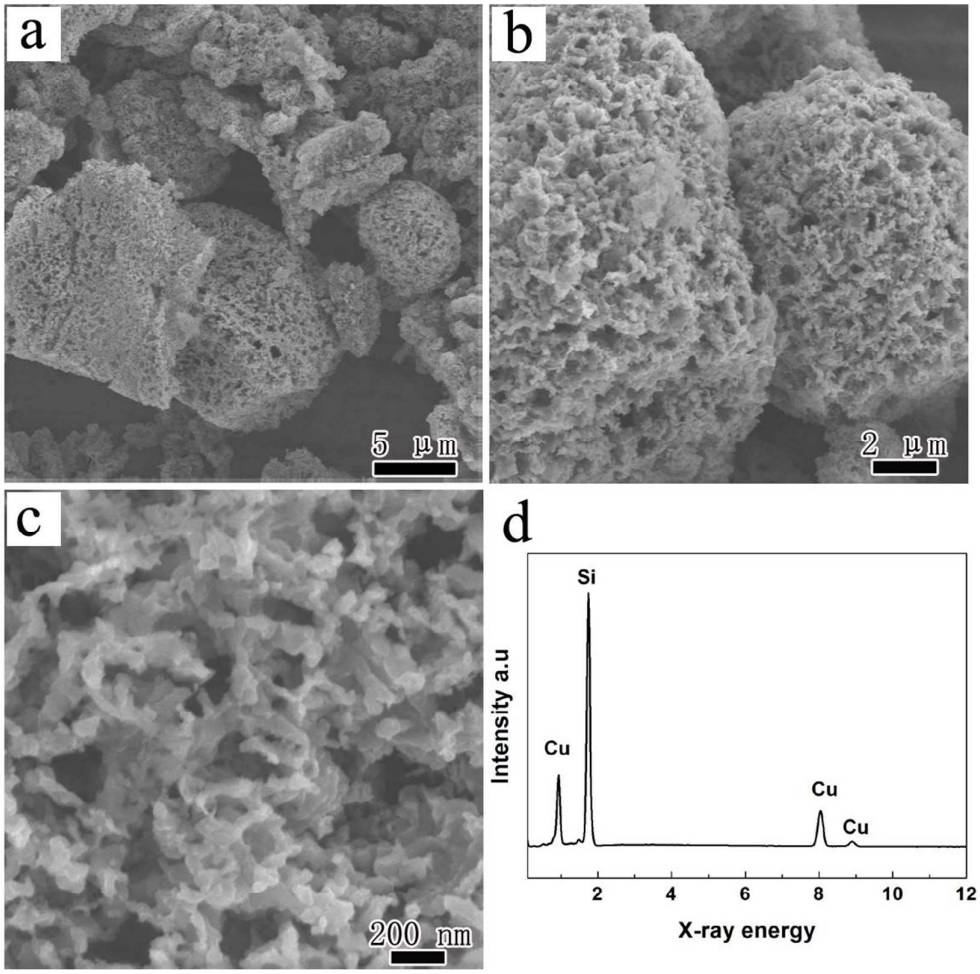

Figure 6. The morphological and compositional characterizations of the bare Si TPS: (a), (b), (c) SEM images; (d) EDX pattern

Journal of Materials Chemistry A Accepted Manuscript

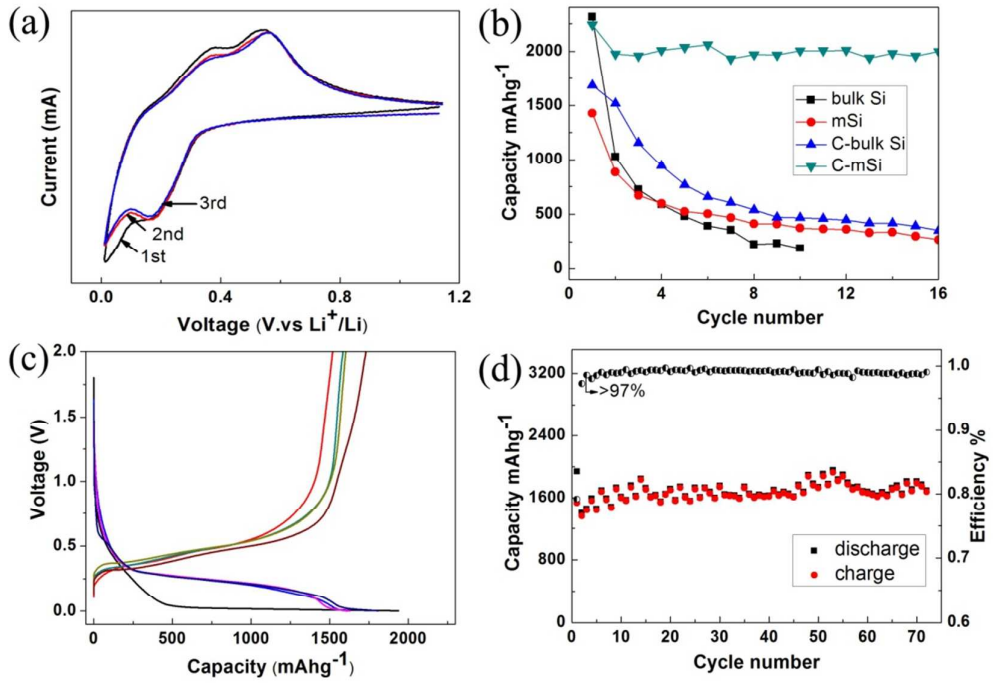

Figure 7. (a) current-voltage (CV) curves for the first three cycles of the Si@C TPS; (b) the capacity versus cycle numbers of the bulk Si, carbon-coated bulk Si, bare Si TPS and Si@C TPS at 0.1 C between 0.001 and 2 V, respectively; (c) the voltage profiles of the Si@C TPS anode at 0.2 C between 0.001 and 2 V; (d) the capacity versus cycle numbers of the Si@C TPS at 0.2 C between 0.001 and 2 V

Journal of Materials Chemistry A Accepted Manuscript

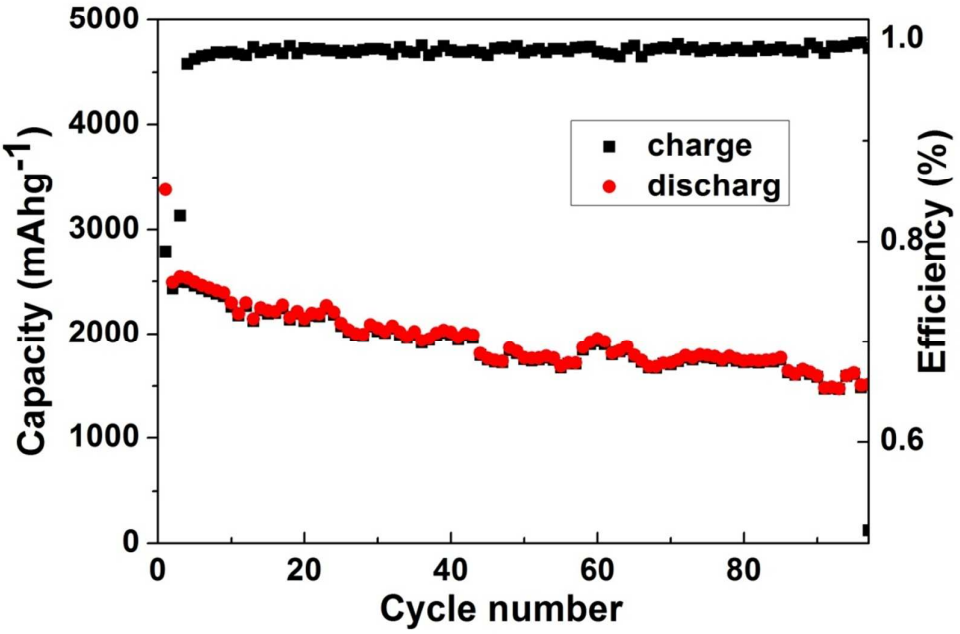

Figure 8. The capacity versus cycle numbers of the Si@C TPS with low carbon content (~8%) at 0.2 C between 0.001 and 2 V

Journal of Materials Chemistry A Accepted Manuscript

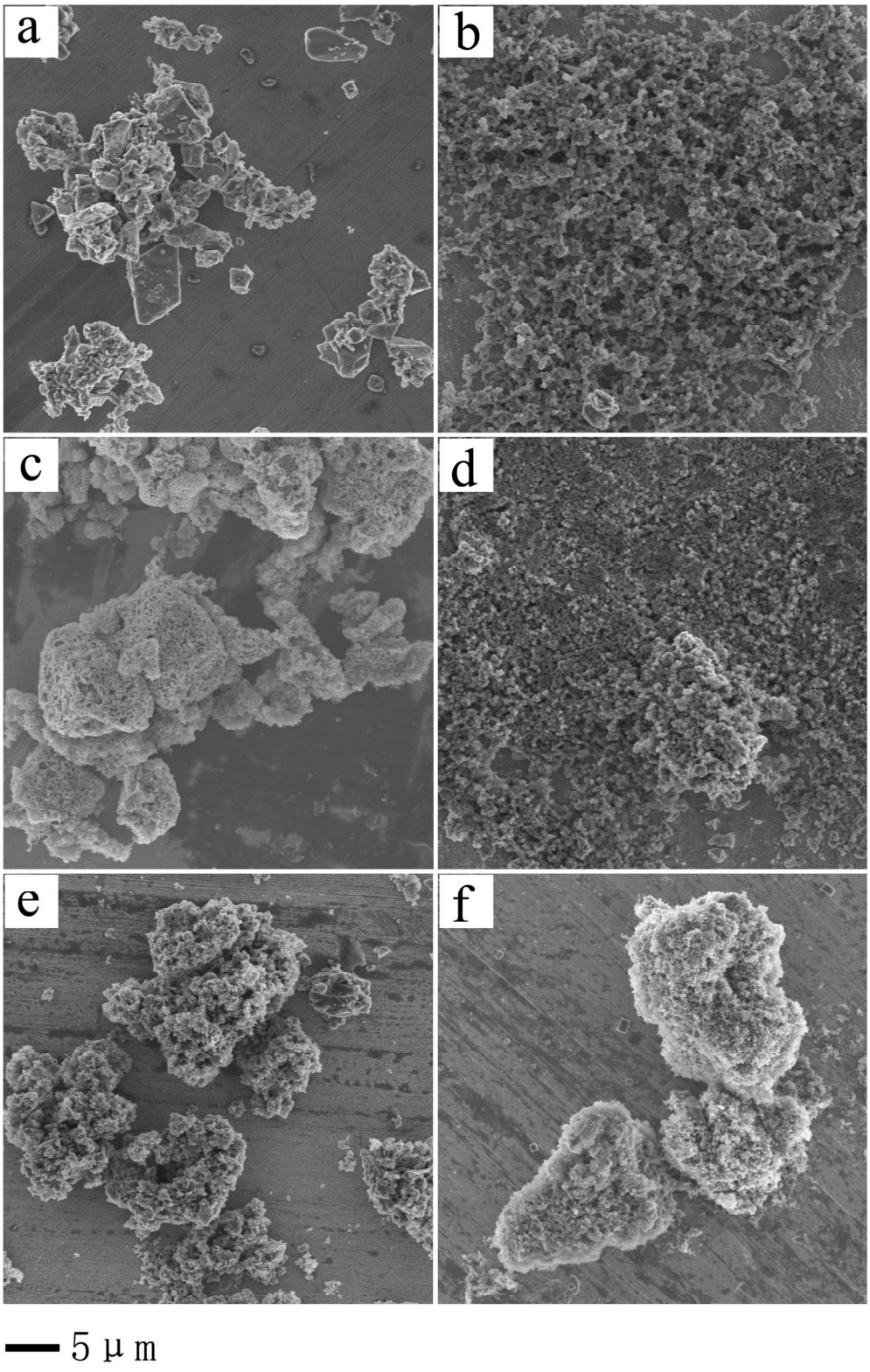

Figure 9. SEM images of the bulk Si (a), (b), bare Si TPS (c), (d) and Si@C TPS (e), (f) before and after cycling

Journal of Materials Chemistry A Accepted Manuscript